Interactive Holographic Stereograms with Accommodation Cues

Quinn Y. J. Smithwick, James Barabas, Daniel E. Smalley, and V. Michael Bove, Jr.
Object-Based Media Group, MIT Media Laboratory, Room E15-368, 20 Ames St., Cambridge, MA USA 02142-1308

ABSTRACT

Image-based holographic stereogram rendering methods for holographic video have the attractive properties of moderate computational cost and correct handling of occlusions and translucent objects. These methods are also subject to the criticism that (like other stereograms) they do not present accommodation cues consistent with vergence cues and thus do not make use of one of the significant potential advantages of holographic displays. We present an algorithm for the Diffraction Specific Coherent Panoramagram -- a multi-view holographic stereogram with correct accommodation cues, smooth motion parallax, and visually defined centers of parallax. The algorithm is designed to take advantage of parallel and vector processing in off-the-shelf graphics cards using OpenGL with Cg vertex and fragment shaders. We introduce wavefront elements – "wafels" – as a progression of picture element "pixels", directional element "direls", and holographic element "hogels". Wafel apertures emit controllable intensities of light in controllable directions with controllable centers of curvature, providing accommodation cues in addition to disparity and parallax cues. Based on simultaneously captured scene depth information, sets of directed variable wavefronts are created using nonlinear chirps, which allow coherent diffraction of the beam across multiple wafels. We describe an implementation of this algorithm using a commodity graphics card for interactive display on our Mark II holographic video display.

Keywords: synthetic holography, 3-D display, holographic video, computer graphics, graphics processors

1. INTRODUCTION

1.1. Motivation

Holographic video offers the promise of the ultimate display with the potential to produce animated autostereoscopic 3-D scenes with all visual depth cues; other 3-D displays offer only a subset. However, due to the large amounts of data required to compute the diffraction pattern for holographic displays, compromises are often made to reduce the bandwidth and computational requirements – horizontal-parallax-only (HPO) and multi-view stereographic display. An HPO display takes advantage of the fact that stereopsis occurs in the horizontal direction due to the horizontal orientation of the human eyes. The information content and computational requirements for rendering for an HPO display are (typically, as a function of the vertical resolution) reduced by several orders of magnitude compared to a full parallax display.

In a multi-view stereographic display, the continuous three-dimensional scene information is approximated by projecting a number of two-dimensional images of the scene into their corresponding view directions either in one dimension for HPO or two dimensions for full parallax. The information content and computational requirements for rendering a multi-stereographic display are greatly reduced compared to a true hologram because only a finite number of scene viewpoints need to be rendered and displayed.

Multi-view stereographic displays provide disparity (binocular parallax) and vergence cues, but generally do not provide (or only approximate, when a large number of views are available) accommodation cues and continuous motion parallax. Both accommodation cues and smooth motion parallax are needed for visually selected centers of parallax. The need for a large number of views places a large computational and physical demand on the display.

Accommodation, motion parallax, and visually selected centers of parallax are useful in reducing the visual clutter in scenes that span significant depth. Motion parallax allows the ability to look around objects and to estimate depth based

on relative motion to a fixated point. Visually selected centers of parallax allow the eye to track a target while the head moves. With accommodation, points at depths other than the plane of focus will be blurred.

Accommodation is a weak depth cue, effective only at distances less than two meters and often coupled with other cues. Due to the difficulties in scaling holographic video displays, current displays are small and used at short distances, precisely where accommodation cues are needed and useful. With advances, large holographic displays with deep scene content are envisioned for possible uses in interactive data visualization and manipulation, where accommodation cues and motion parallax are needed and useful.

In a multi-view stereogram, motion parallax occurs in discrete steps. Objects of interest need to be visually reacquired as one viewpoint changes to another. Also, in a multi-view stereographic display, the viewer verges on an object but accommodates either at infinity or at a screen. Normally, vergence and accommodation are coupled in the human visual system. The uncoupling of the accommodation and vergence cues reduces stereoacuity and increases time to identify stereoscopic stimuli, and may also cause fatigue and even nausea when viewed for long periods and at short distances.[1]

Our goal is to reintroduce the accommodation cues and smooth motion parallax into holographic multi-view stereograms (also called parallax panoramagrams) with appropriate wavefront reconstruction, while maintaining the benefits of spatial and view sampling for information reduction, and the ability of rapid computation from parallel computation of certain classes of multi-view stereogram algorithms.

To this end, we develop the Diffraction Specific Coherent Panoramagram (DSC Panoramagram), composed of an array of wavefront elements ("wafels") to control the intensity, direction, and center of curvature of light. With controllable wavefronts, fewer views are needed to provide the accommodation cues and smooth motion parallax. The DSC Panoramagram is an extension of the Diffraction Specific Stereogram[2] and Reconfigurable Image Projection (RIP) implementations[3] with a more flexible and complete set of holographic basis functions (variable rate chirps) computed on-the-fly. The algorithm's parallel-vector computations and the programmable pipeline of modern GPUs allows the DSC Panoramagram to be computed in real-time.

1.2. Background

In a fully computed hologram, such as a Fresnel hologram, every point in a 3-D scene contributes to every point in the holographic fringe pattern (ignoring occlusion). Such a hologram is typically computed via the intereference between the points' spherical wavefronts and a reference beam. In comparison, the stereogram can be considered an array of Fourier transformed perspective views of the scene, although it may be implemented in a variety of methods.

Stereograms, such as in lenticular, integral, or holographic stereogram displays, can be created using arrays of direls or hogels. Whereas a pixel ("picture element") emits light equally in all directions, a direl ("directional element") emits a controllable intensity of light in each direction. A direl is a point emitter, and therefore must emit a spherical wave with a fixed center of curvature. A hogel ("holographic element") emits controllable intensity of light in a set of directions as plane waves. A direl array can be produced by overlapping holographic chirp lenslets, where as a hogel array is typically implemented using abutting combinations of fixed pitched gratings. The chirps and gratings are amplitude modulated by view data to produce viewzones. We extend the pixel, direl/hogel progression to the "wafel" – a wavefront element which emits a controllable intensity of light with a controllable wavefront curvature in each direction. A wafel uses diffractive chirp lenslet segments each of whose focus depends on the scene depth. A wafel must be an extended area to emit arbitrary wavefront curvature. Wafels can also be abutted to create larger coherent wavefront supports. See Fig. 1.

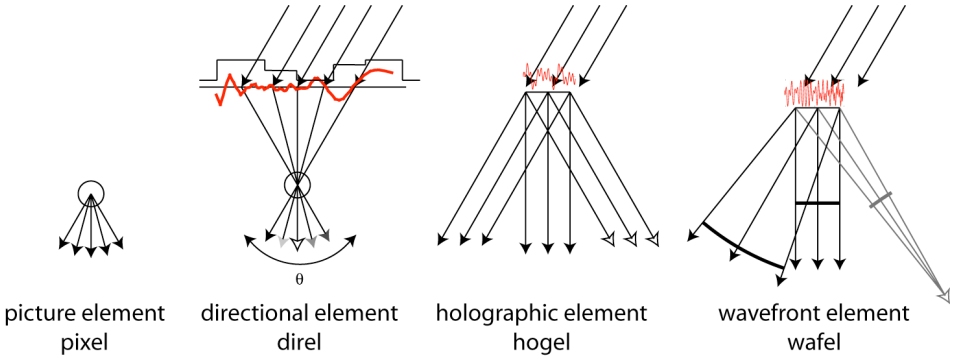

Fig.1. Pixel, Direl, Hogel, Wafel progression.

1.3. Stereograms vs. holograms

Yamaguchi, *et al.*[4] have investigated the theoretical differences between a holographic Fourier stereogram and a Fresnel hologram. The Fresnel hologram expresses three phase terms in its wavefront related to direction, depth, and nearby points on the hologram. A holographic stereogram expresses only one phase term related to direction. This implies that a holographic stereogram has a lower resolution for objects far from the hologram plane and will not approach the quality of a Fresnel hologram even for large numbers of views. The additional phase terms provide the phase relationship (coherency) among stereogram array elements, continuous direction and wavefront curvature. In order to better approximate an arbitrary wavefront, variable curvature at the hologram plane and coherency between apertures need to be included.

A stereogram approximates an arbitrary wavefront using either a set of plane waves or a set of spherical waves of constant curvature at the hologram plane in a set of discrete directions. To begin with, for an adequate approximation more than one set of views from the same point must enter the eye's pupil, requiring a large number of views over the display's field of view. More than 170 views over a 30° field of view (FOV) are needed for two views to enter a 4 mm pupil at a 0.65 m viewing distance.

Since wafels produce segments of spherical wavefronts with variable centers of curvature emitted in controllable directions, wafels can better approximate segments of the ideal wavefront. Fewer views are needed for accurate arbitrary wavefront reconstruction.

1.4. Chirp splicing

When considering the holographic fringe composition, a similar conclusion about the difference between holographic stereograms and fully computed holograms can be found. Holographic stereograms splice together segments of chirps from different direls to approximate the ideal chirp of a hologram that produces a point at an arbitrary distance. The direl chirp segments are amplitude modulated by view data and form the views of the direl. For points behind the emitter plane, the ideal chirp is approximated by a combination of chirp segments with opposite chirp rates. This implies that for a better approximation, the chirp segments should be made extremely short. Therefore, more views are needed for a better approximation of the correct chirp. However, even in the limit, the approximation may not equal the true chirp because the chirp rates of the approximating chirps may be opposite of the true chirp.

In contrast, the Diffraction Specific Coherent Panoramagram (DSC panoramagram) consists of an array of wafels. The array of wafels samples the scene in space and angle then computes chirps that are segments of the ideal chirp. A large number of views are not needed to approximate the wavefront curvature, as each segment is the appropriate curvature. As the sampling in space and angle increase, in the limit, the stereogram with accommodation cues will converge to a fully computed Fresnel hologram, and the many-to-many computations reemerge as every scene point contributes to every point on the hologram. See Fig. 2.

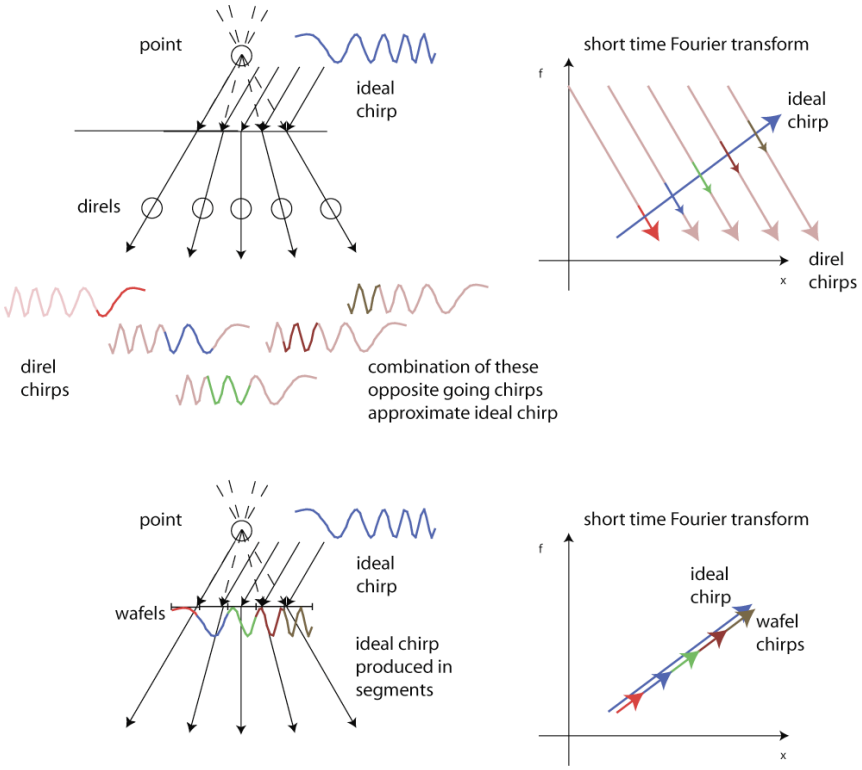

Fig. 2. Chirp splicing -- holographic stereograms with direls (top) and wafels (bottom).

1.5. Accommodation cues

For accommodation, the monocular eye changes the focal length of the lens to merge a continuum of multiple images of the object coming from different directions into a single image, as well as to make the wavefront converge to a point on the retina. For a physical object point, these two conditions are naturally met together; however in a stereogram, they do not occur together.

In an idealized consideration, a stereogram seems to readily produce these accommodative cues because the view projections are ideally rays that cross at scene points. Upon entering an eye focused at a scene point, the scene point should be imaged with all rays from that scene point converging to a sharp point on the retina. See Fig. 3a. For an eye out of focus, the rays converge before or after the retina to form a blurry point. See Fig. 3b. In reality, the view projections are wavefronts approximated by ray bundles and there are a finite number of views. A set of bundles related to a view form a view image. For an eye focused at a scene point, the central rays of the view ray bundles cross at the retina but the remainder of their rays (and wavefronts) converge other locations. The multiple view images overlap on the retina, but they are in focus at another location. A blurry spot is seen. See Fig. 3c. For an eye focused at infinity, each set of ray bundles (and wavefronts) converge at the retina, but their central rays do not cross there. The views focus to individual points on the retina. Multiple sharp points are seen. See Fig. 3d.

In a stereogram with coarse sampling of space and angles, a scene point may not be seen from adjacent wafel apertures, even without occlusion. For points away from the wafel plane, each view may be seen as separate discrete image. This is called “interperspective aliasing” and is related to the sampling of a point's parallax viewed from the apertures. Typically, the number of views is increased or a depth-dependent blur (anti-aliasing) is applied so multiple images are overlapping or abutting in a desired depth range. The filtering will remove the chirp discontinuities producing a smooth wavefront but will produce a distribution of points.

In a DSC Panoramagram, the convergences of the object’s view images and the segmented wavefront to a point on the retina naturally occur together. See Fig 3e-f. Wafels reconstruct portions of wavefonts with variable centers of curva-

ture and hence form real and virtual points. When the eye is focused at the scene point, all the view images of the point will converge and the wavefronts from different wafel apertures will collapse to a single point; the point is coherently imaged. If there are too few view samples, inter-perspective aliasing still occurs. However scene points not at the focal plane may exhibit aliasing (multiple images) but will be blurry, so will contribute less to the perceived image. The eye is accustomed to seeing multiple blurred images ("double vision") away from the focal plane, as this occurs (but is an unrelated phenomenon) in stereo vision. Increasing the number of views increases the sampling of the point's parallax and decreases the gaps in the point's blur. Distance can be estimated by the blur gradient -- the rate of blurring around the point of fixation.[5] The blur gradient is not correct for stereograms, but is for panoramagrams.

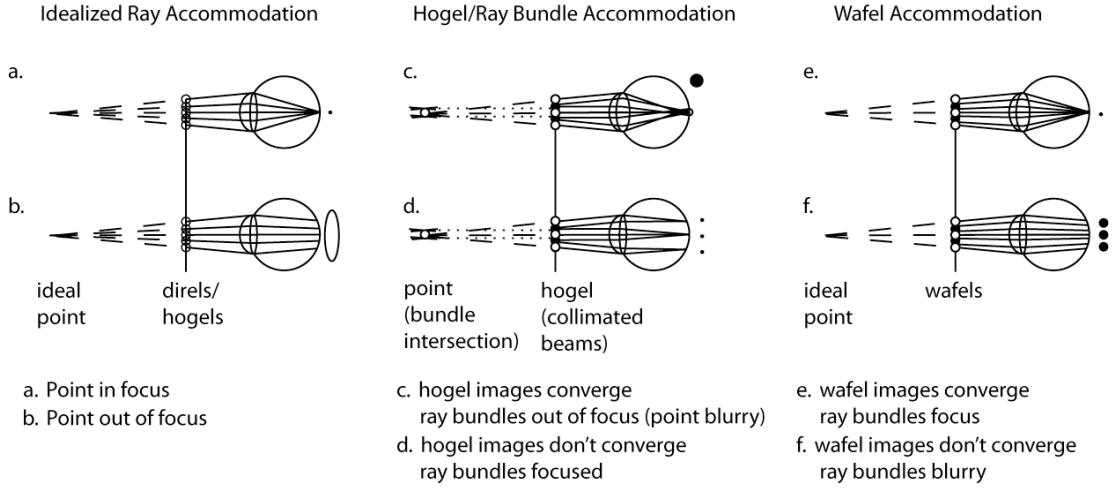

Fig. 3. Ideal, direl/hogel in stereograms and wafel accommodation in DSC panoramagram.

1.6. Motion Parallax and Accommodation

Multi-view stereograms also allow for motion parallax depth cues, however the parallax may appear unnatural with a small number of views and without accommodation cues. The discreteness of views can be apparent and parallax occurs in steps. For multi-view stereographic displays, a large number of views are required for smooth view changes and to make the object appear to occupy a definitive location and orientation in space; at least two views need to enter the pupil.

Head tracked autostereoscopic displays provide dense, smooth view changes for a single user and exhibit continuous motion parallax. However, these displays cannot track accommodation so the parallax plane is typically programmed to be at the screen surface. The viewer cannot visually choose the parallax plane by fixation as naturally occurs.

Smooth view change, as well as the ability to focus at different depths, makes it possible for the viewer to choose any depth plane as a parallax plane. This process can be done with binocular or monocular vision, so vergence is not necessary, although helpful. The viewer can accommodate and verge on a single scene point at any depth while moving the viewing position. Objects and points behind the tracked point will appear to move in the opposite direction as objects in-front of the viewer's fixated point, and the amount of movement will depend on the depth of each point. Without the smooth view changes, parallax will be constant as the eye travels in a single view zone. Parallax will discretely change as the eye moves from one view to the next. Accommodation is naturally involved in discriminate depth, decluttering a scene, and tracking objects.

Since wafels reconstruct portions of wavefonts of real and virtual points, smooth motion parallax at visually chosen parallax planes will naturally occur even for few views. With smooth motion parallax, the brain can extrapolate motion across discontinuities in the views due to occlusion or inter-perspective aliasing.

1.7. Goals of this work

Using a wafel's ability to emit controllable wavefront curvature in a variety of directions, we can decouple the accommodation cues from angular sampling of the scene. Similarly, large numbers of views are not required for wavefront approximation, accommodation and smooth motion parallax. For wafels, increasing the number of views increases continuity of parallax, contiguity of blur spots, and updates of angle dependent shading (specular highlight and iridescence). Increasing the number of wafels in the hologram increases the spatial sampling of the scene and thereby the pixel resolution of each view and occlusion updates. The correct wavefront is generated for all viewable points in the scene. The wavefronts exhibit continuous direction, phase coherence between multiple sampling apertures, and correct centers of curvature. Focused virtual and real points are created, not approximated by intersecting ray bundles. The chirp fringe pattern to generate the desired wavefront is the correct pattern across multiple wafel apertures, not an approximation from chirp segments generating fixed constant curvature wavefronts. Binocular vergence and monocular convergence are consistent, and vergence and accommodation are recoupled (at least in the horizontal direction for HPO displays).

In following sections of this paper we proceed to derive the equation of the wafel's chirps, formulate the rendering algorithm, implement the algorithm on a holographic display, and perform simple experiments to assess qualities of the displayed hologram.

2. FORMULATION

2.1. Sampling

Our formulation is a natural extension of diffraction-specific holographic stereogram rendering algorithms developed at the MIT Media Lab. Diffraction-specific holographic stereograms (DSHS) concentrate on wavefront reconstruction via fringes rather than on emulating the physical process of interference.[2] They are equivalent to discretizing the hologram in space and spectrum (*i.e.* frequency content or angular deflection). These algorithms are image based techniques, so they naturally capture occlusion, texture and lighting. In the general instantiation, hogels composed of fixed pitch gratings amplitude modulated by captured scene imagery send light in the various directions with flat wavefronts.[6] Hogels and their fringe basis functions can be more general and complicated than this, being iteratively computed to satisfy desired spatial and spectral constraints and produce scenes from 3D point locations. Here we consider the general implementation to produce stereograms from view imagery and hogels that project directional views at infinity. This allows the same precomputed basis functions to be used for all hogels, which also implies fringes will not be coherent across hogels. In the Reconfigurable Image Projection (RIP) algorithm,[3] overlapping precomputed chirped gratings modulated by scene imagery create point emitters (direls) with spherical wavefronts of a fixed center of curvature. We previously formulated a parallelized vector version of the RIP algorithm.[7]

Plesniak, *et al.* suggested various volumetric embodiments of the RIP algorithm with direl emitters (or points) located in arrays at multiple planes or emitters conforming to the surface of objects. Presumably, this would allow for accommodation cues. For each point, a scene modulated depth-dependent chirp would be created in the hologram. Multiple chirps would be blended to form the hologram. Handling occlusion becomes difficult and removes one of the benefits of image based algorithms. In the conformal emitter case, holographic rendering is scene dependent and the potential number of emitters unbounded.

One of the difficulties of spatial and angular sampling from arbitrary locations is that the footprint of the chirp on the hologram plane depends on the depth of the point. If we capture views from a location in front of the hologram plane, as in the RIP algorithm, the views and chirps need to be projected onto the hologram plane. This makes it difficult to perform the calculations in a parallelized way, since the footprint on the hologram plane is depth dependent. We can't tell beforehand which scene points and views contribute to a point on the hologram.

To solve these issues, we develop the Diffraction Specific Coherent Panoramagram. To create the hologram, an array of wafels is created, each sampling the scene's intensity and depth in a set of directions from the center of each wafel aperture. The wafels sample the scene at the hologram plane, so the footprint for each view is defined to be the width of the

wafel's aperture. This also means we sample the hologram in space and spectrum. Note that for the horizontal parallax only case, the wafels form a vertical stack of 1-D horizontal wafel arrays. Each array samples over the set of horizontal directions but with the vertical perspective located at the viewer's eye away from the hologram. The equivalent camera would be astigmatic, with two centers of projection. The full parallax hologram consists of a planar 2-D array of wafels sampling the scene in both directions. From the scene point's depth sampled for a given position and angle, a chirp is computed across the wafel aperture to produce a wavefront that emanates as if it is from that observed point. A continuous coherent chirp can be computed from abutting apertures that see the same point. The chirp's support varies with the distance of the point to the hologram plane. See Fig. 4. Chirp segments related to a point will still be coherent even if the point is partially occluded or not viewed from some apertures.

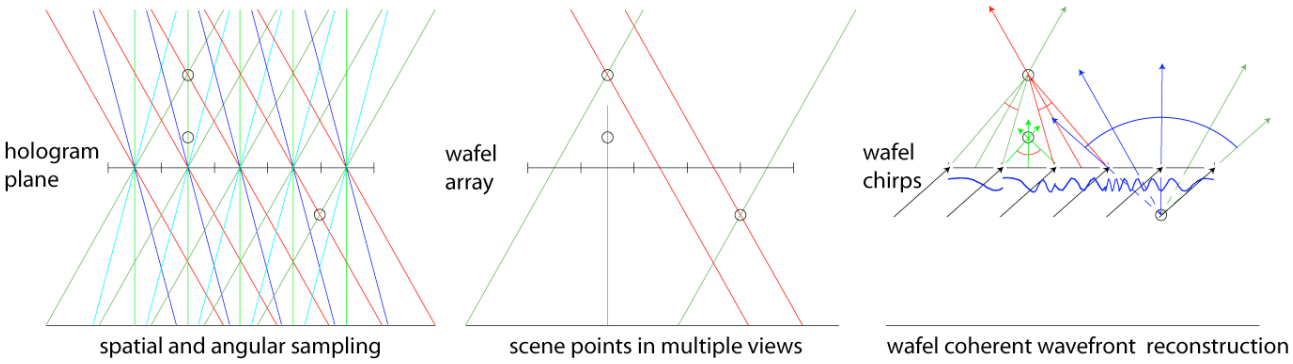

Fig.4. Spatial/angular sampling and coherent wavefront reconstruction with wafels.

The chirp segments that create a point focus must be computed for each wafel independently from other wafels, since individual points are not tracked and neighboring wafels may not see the same point due to occlusion or angular sampling. The chirps must be computed only from their wafel position, a view angle, and a depth value. Wafels generate wavefronts that originate only from points that are seen from the array in the fixed directions. A fixed maximum number of points are generated. Occlusion is naturally handled, since an occluded point will not be seen from some apertures, but will from others.

2.2. Mathematical derivation

The equation of the wafels' chirps can be derived by first determining the instantaneous frequency of a diffractive grating at a point on the hologram required to diffract light to a desired point:

$$f = \frac{1}{\lambda}\left(\frac{x - x_0}{\sqrt{(x - x_0)^2 + {z_0}^2}} + \sin\theta_r\right) \tag{1}$$

Where x is the horizontal position in the hologram, x_0 is the horizontal position of the scene point, z_0 is the depth of the point in the z-direction, θ_r is the angle of the reconstruction beam, and λ is the wavelength of the illumination.

The argument of the chirp's cosine function, Θ, is found by integrating the instantaneous frequency (1) with respect to the hologram position, x, with the constant of integration chosen so the chirp's phase is zero directly under the desired point, $x - x_0 = 0$.

$$y = \cos(\Theta) = \cos\left(\frac{2\pi}{\lambda}\left(\sqrt{(x - x_0)^2 + {z_0}^2} - z_0 + x\sin\theta_r\right)\right) \tag{2}$$

The square root term will produce a chirped frequency that depends upon the depth of the point (or radial distance). The z_0 term will produce a phase shift so the chirp's phase contribution is zero directly under the point, $x - x_0 = 0$. The $x\sin\theta_r$ term will produce a constant frequency grating related to the input angle of the reconstruction beam. Fi-

nally, the position of a scene point seen by the wafel, x_0, is computed from the position of the wafel's center on the hologram plane, x_w, the wafel's viewing angle θ_w, and depth of the scene point, z_0:

$$x_0 = x_w - z_0 \tan(\theta_w) \tag{3}$$

Substituting (3) into (2), we get the equation for the chirped grating that produces a diffractive lenslet focusing to the point at depth z_0 seen by a wafel at position x_w, viewing at angle θ_w.

$$y(x_w, \theta_w, z_0, \theta_r, \lambda) = \cos\left(\frac{2\pi}{\lambda}\left(\sqrt{(x_w - z_0 \tan\theta_w)^2 + z_0^2} - z_0 + x \sin\theta_r\right)\right) \tag{4}$$

The chirp pattern in (2) is equal to the 1-D bipolar intensity holographic fringe pattern of a point source.[2] A 2-D chirped zone pattern would also be equal to the 2-D bipolar intensity fringe pattern. Whereas we derived the chirp pattern from a diffraction grating viewpoint, the bipolar intensity was derived from the physical interference between an object wavefront and a reference beam and then excludes the object self-interference and the reference-bias terms. The grating viewpoint derivation is useful because it gives us the instantaneous frequency (1) at each point on the chirp, which will allow us to prevent aliasing when sampling the chirps on the hologram plane.

Furthermore, from (4), the fringe value can be computed for any point on the hologram independently from any other, knowing the wafel's position and rendering view angle and depth of the point from the scene depth map. This will allow the equation to be computed in parallel for every portion of the hologram. The chirp's coherence is maintained across spatial sampling of the scene.

2.3. Other related work

Although the approach, formulation and implementation are different, the final result is similar to work done by Yamaguchi, *et al.* on Phase Added Stereograms (PAS)[4] and Yoshikawa, *et al.* on Coherent/Integral Stereograms.[8] This is understandable and expected, since all spatially and spectrally segment the hologram. With PAS, Yamaguchi acquired 2-D image projections of the scene and added the phase term related to the depth of the object into the holographic stereogram computation. However, Yamaguchi's algorithm is performed in the frequency domain and is implemented using the FFT. Since an FFT is used, there are discrete angles and no curvature. Coherent Stereograms use 3-D image points of the scene and added phase terms related to the depth of the object in the frequency domain holographic stereogram computation, and can represent curvature and arbitrary angles. Occlusion and lighting effects for Coherent Stereograms are not discussed.

In our approach, the formulation and implementation of the Diffraction Specific Coherent Panoramagram are performed in the spatial domain using variable chirps and are an extension of the diffraction specific holographic rendering algorithms. Our formulation uses 2-D projections and depth maps of the scene. Our GPU implementation takes advantage of the vector and parallel nature of the chirp computation. Working in the natural spatial domain of the GPU rendering, the algorithm provides inter-aperture phase, continuous direction and wavefront curvature, as well as providing natural occlusion and lighting information.

3. IMPLEMENTATION

3.1. Methodology

Diffraction specific algorithms consider every point in the hologram to be a summation of view modulated chirps. This can be interpreted as a dot product of a view vector with components from captured scene view intensity, and a chirp vector with components of chirp values that project the scene image in the appropriate direction. The chirp values are computed based on captured scene view depths.

For HPO holograms, the view intensity and depths are sampled only in the horizontal direction and the chirp values computed using (4). For full parallax, the view intensities and depths are sampled in the horizontal and vertical directions, and chirp values are computed based on the 2-D continuous zone plate version of (4).

We implemented the Diffraction Specific Coherent Panoramagram algorithm for the MIT Mark II holographic display.[9] We use C, OpenGL, and NVIDIA's Cg shader language running on a single NVIDIA GeForce GTX260 on an Ubuntu based PC. The view capture, basis computation, and fringe computation is independent of the hardware implementation, but the frame buffer format of the Mark II must be considered.

For the Diffraction Specific Coherent Panoramagram algorithm, we wish to maintain the parallelized vector characteristics of the previous algorithm. In the experiments discussed here, we create an array of 512 by 144 holographic emitters with 16 views (recall that in the proposed method, far fewer views are needed than in a standard stereogram). A horizontal sheared orthographic and a vertical perspective projective view is rendered for sixteen views directly into the appropriate vector format. Because wafels abut, here the appropriate vector format consists of each component being a successive rendered view from the wafel. The shearing plane and holographic plane are coincident, so the chirps do not need to be projected from the image capture plane to the hologram plane. The shearing/hologram plane is in front of the vertical viewpoint and allows points in front of and behind the hologram plane to be captured. The shearing automatically moves the horizontal position of the perspective viewpoint. The vertical perspective divide is done in a vertex shader. Each view is rendered into a single color channel. Since GPUs typically use four component vectors, sixteen views are stored as four 4-vectors tiled vertically. Depth is similarly rendered either concurrently into a separate render target or sequentially in a second pass, aligned and tiled vertically with the corresponding view render. For an orthographic projection, the z-coordinate is not transformed and is linear in depth. These images are stored as 16-bit textures to provide fine depth resolution. See Fig. 5. A screen aligned polygon that vertically spans two heads of a single graphics card is then rendered (2048x3514 pixels). For each head, the fragment shader divides the vertical coordinates amongst a single vertical blanking header of 356 lines, and eight data sections of 128 lines with an additional 50 horizontal blanking lines at the before of each data section. Each data section is a single holographic line of 262144 pixels. The fragment shader then divides the active data section into 512 wafel apertures. Each wafel aperture's normalized horizontal coordinate is then divided into 512 pixels. Due to the bi-directional scanning, every other data line is reversed.

For each fragment belonging to a data line, the fragment's hololine position is computed from the wafel number and the wafel normalized coordinate. From the hololine position, the corresponding view and depth vectors are fetched. The benefits of rendering into the natural format is that scaled normalized coordinates for the hololine, view, and depth textures are aligned and their tiled vectors are simple offsets, making texture fetches easy to compute and coordinate. Another benefit of rendering into the natural format is that the view and depth vectors do not need to be assembled from scattered components, saving computation and texture fetches. From the hololine position and the depth vector, the chirp vector is computed. The fringe value is simply computed as dot products of the view vector and the chirp vector.

Because we sample the hologram, aliasing needs to be addressed. If a fringe spacing finer than twice the sampling required to deflect to a desired angle, aliasing/folding may occur. Fortunately, we can calculate the diffraction angle at each fragment using (1). If the maximum diffraction angle is exceeded, meaning aliasing will occur, the fragment can be excluded from the fringe pattern.

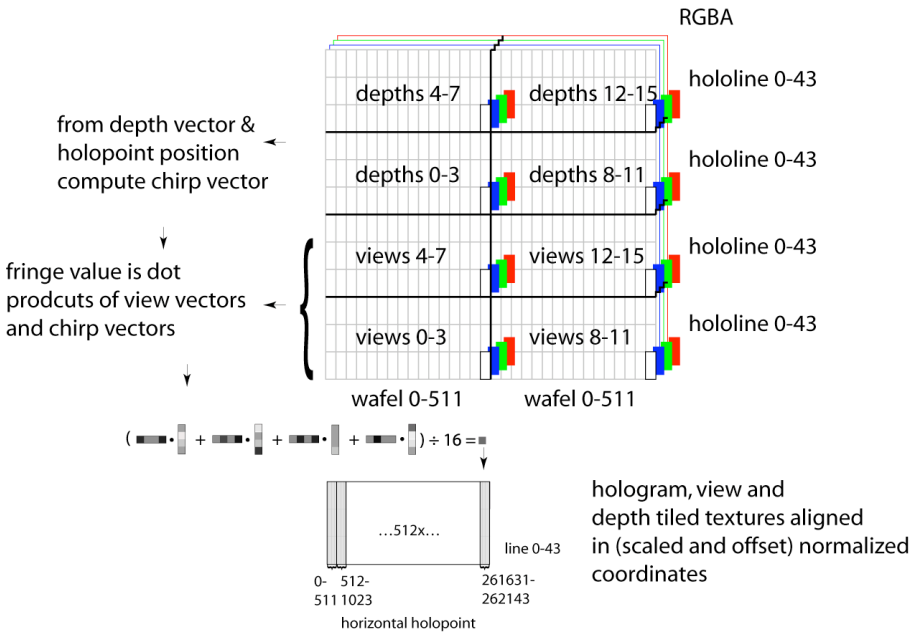

Fig. 5. View and depth format and fringe computation.

3.2. Focus experiment

Holograms of a pair of vertical lines were created on the Mark II holovideo display to investigate the ability of the Diffraction Specific Coherent Panoramagram to provide accommodation cues, smooth parallax, and visually chosen parallax planes. The display is horizontal parallax only, and the use of vertical lines allows us to concentrate on these effects only in the horizontal direction.

For comparison, we modified the fragment shader to compute a multi-view stereogram using hogels. The variable chirps of the DSC Panoramagram were replaced with a set of constant pitch gratings to diffract the image modulated light into the appropriate views but without focusing.

To provide a gold standard for comparison, we also generated a Fresnel hologram of the pair of vertical lines. The Fresnel hologram is implemented in the fragment shader using horizontal and depth coordinates of line to compute the diffraction pattern. The Fresnel hologram does not include occlusion effects.

We used a Canon EOS camera approximately 0.4 m away from the hologram plane to capture images of the lines' holographic reconstructions on the display. The camera settings were chosen to photograph the display rather than to emulate the human viewing conditions. The two lines are displaced horizontally and in depth: Line 1: $(x_0, z_0) = (-10$ mm, $+1$ mm), Line 2: $(x_1, z_1) = (0$ mm, $+20$ mm), with z distances measured from the hologram plane. The Fresnel hologram is displayed and the camera focused on the front line (Line 1) and an image captured (Fig. 6a). The camera is then focused on the rear line (Line 2) and an image captured (Fig. 6b); likewise for the Diffraction Specific Coherent Panoramagram (Figs. 6c and 6d). The Stereogram is displayed and the camera is focused on the image plane where the multiple images are the sharpest (Fig. 6e). Then the camera is focused where the projections of Line 2 cross, corresponding to the focus of the front line (Fig. 6f).

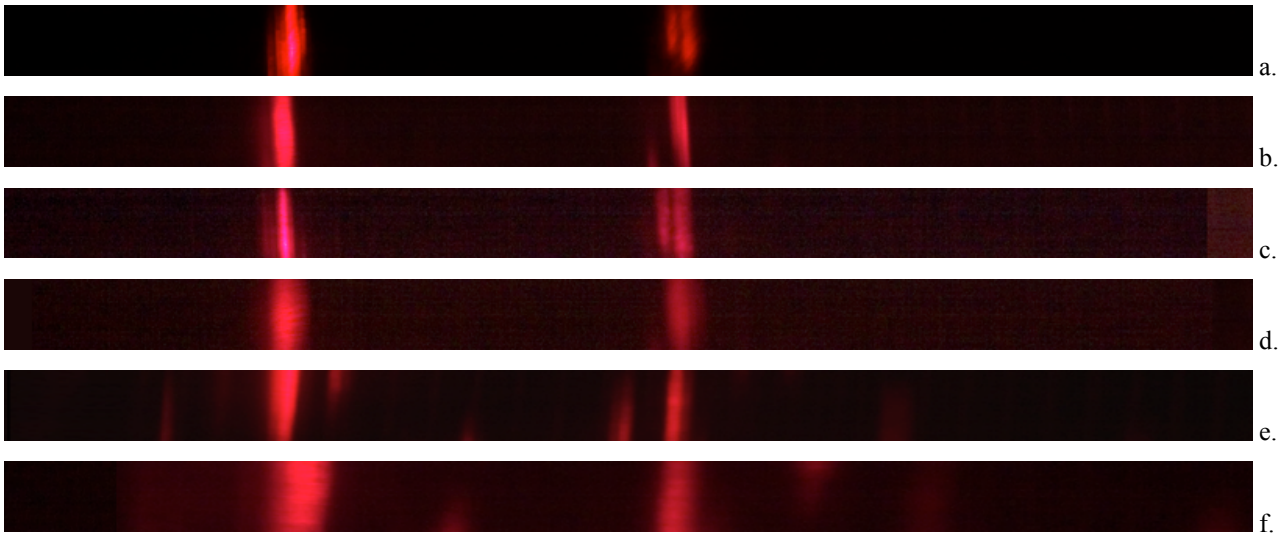

Fig. 6. a. Fresnel hologram focused on first line, b. Fresnel hologram focused on second line, c. Paroramagram focused on first line, d. Panoramagram focused on second line, e. Stereogram focused on first line, f. Stereogram focused on second line.

3.3. Smooth motion parallax experiment

To test for smooth parallax changes, two lines are displaced horizontally and in depth: Line 1: $(x_0, z_0) = (-10$ mm, +1 mm), Line 2: $(x_1, z_1) = (0$ mm, +40 mm). The separation of the two lines in depth was increased here to provide greater parallax. We visually fixate on front line (Line 1) and translate our heads to observe the relative motion of the lines, then repeat while visually focusing on the other line (Line 2). For smooth parallax changes we look for the absence of discrete view changes or "ratcheting."

3.4. Visually-defined parallax planes experiment

To test for visually defined parallax planes three lines are displaced horizontally and in depth: Line 1: $(x_0, z_0) = (-10$ mm, +1 mm), Line 2: $(x_1, z_1) = (0$ mm, +10 mm), Line 3: $(x_2, z_2) = (+10$ mm, +20 mm). For visually defined parallax planes, we look to see if the fixated line remains stationary while the other line moves relative to the fixated line. Lines in front of the fixated line should move together and in the opposite direction of lines behind the fixated line. This is done for the Fresnel hologram, the Diffraction Specific Coherent Panoramagram, and the stereogram.

3.5. Results

Examining the figure pairs (Fig. 6a/b and c/d), the lines are in focus at different focal planes for both the Fresnel hologram and the Diffraction Specific Coherent Panoramagram. The stereogram lines only focus at one focal depth and there are a couple of sharp view images for each line (Fig. 6e). Focusing the camera at a different plane causes the paired view images to converge leaving blurry single lines (Fig. 6f). This is as expected and shown in Fig. 3. In the panoramagram's Fig. 6c, there is a extraneous dim line next to out-of-focus Line 2. This is not an inter-perspective aliasing artifact because the extraneous line also occurs in the Fresnel hologram. However, the additional lines in the stereogram's Fig. 6e are likely inter-perspective aliasing because it occurs for both Line 1 and Line 2 and appears sharp on the image plane where the other line images are focused.

Visually, for both the Fresnel hologram and the panoramagram, the difference in accommodation between lines is difficult to appreciate, as it is rather subtle. The depth of field of the human eye is 0.3D for a 4 mm pupil.[10] For a viewing distance of 0.6 m, the depth of field is 130 mm behind and 90 mm in front of the screen. Our lines are about 20 mm apart at about 0.6 m, chosen because of display aberrations. When focusing on the front line, the separate view images of the back line may be sufficiently in focus.

Also, the total usable depth of our display is about 170-180 mm due to astigmatism common to all HPO displays. It is

typical to regard the usable depth of field of an astigmatic hologram to be bounded by 0.25 diopter of astigmatism,[11] which for a viewing distance of 0.6 m, is 100 mm behind and 78 mm in front of the display. So the depth of focus of the eye is about the full depth of the display at the normal working distance. This may mean that accommodation cues provided by the DSC Panoramagram will be more beneficial for large full-parallax displays with large depth variations, or possibly smaller close-work (0.3 m to 0.6 m) displays where focusing cues change rapidly. The latter case may be important for interactive holographic displays with haptic devices.[12]

Also, display scanning artifacts and aberrations are apparent and distracting. For both the Fresnel hologram and the DSC Panoramagram, the front line (Line 1) is broader with halos even when in focus, while the back line (Line 2) appears very sharply in focus in both cases. The display optics are likely out of alignment causing the broadening of the front lines. The halos are likely caused by noise (or over modulation/saturation) in the support of the holographic chirp. Considering that the Fresnel hologram and DSC Panoramagram look similar to each other, but different from the stereogram, the results are a validation of the DSC Panoramagram.

Both the Fresnel hologram and the DSC Panoramagram provide smooth motion parallax over the FOV of the display, without any apparent discrete view changes or ratcheting within a single viewzone or adjacent viewzones where the object is still seen. The apparent horizontal spacing between the two lines separated in depth varies almost continuously as the eye is translated horizontally. In comparison, the stereogram's discrete views are apparent and parallax occurs in steps. The apparent horizontal spacing between the two lines separated in depth seems constant within a single viewzone, then the spacing discretely changes as the eye moves into the adjacent viewzone.

We could visually choose parallax planes for both the Fresnel hologram or the DSC Panoramagram. However, glare and reflections off the vertical diffuser surface often draws the eye's attention, and accommodation occurs at the screen rather than the desired point. When this occurred, the plane of parallax changed with placement of the vertical diffuser. Visually choosing the parallax planes with the stereogram was difficult, if not impossible, using either one or both eyes to fixate. The discrete view changes and discrete parallax made it necessary to consciously refixate after moving into a new viewzone.

Perceptual and performance experiments are ongoing and we expect to publish more complete results in the near future. In addition to test stimuli, we have also rendered texture- and normal-mapped objects with lighting and occlusion as DSC Panoramagrams. A 500-polygon scene was generated by non-optimized software at 42 frames/second, while for comparison the same scene rendered as stereograms using hogels ran at 78 frames/second.

4. CONCLUSIONS

Diffraction specific holographic rendering algorithms were developed to increase the speed of holographic computation for real-time holovideo displays by concentrating on wavefront reconstruction via precomputed fringe basis functions. In the original implementation, hogels discretize the hologram in space and spectrum. While other basis functions could be used for hogel generation, the general approach was to use a combination of optimized fixed pitched gratings producing directional planar wavefronts to place the viewing location at infinity.[13] This allowed the same set of precomputed basis fringes to be used for all imagery.

The Diffraction Specific Coherent Panoramagram generates depth-dependent chirped gratings on the fly from scene image and depth data to generate wafel arrays with directional sections of spherical wavefronts with variable centers of curvature. These wavefronts were chosen to provide useful accommodation cues, smooth motion parallax, and visually defined parallax planes without the approximation from using a large number of views. Unlike conventional stereograms, the DSC Panoramagram converges to a Fresnel hologram in the limit of increased view and spatial sampling.

Our main extension is how to use parallel computation to generate chirped gratings coherent across multiple apertures based upon view samples of the scene at different wafel locations along the hologram. The chirped gratings' supports are not confined to a single wafel aperture.

The DSC Panoramagram algorithm is designed for parallel vector operations suited for efficient implementation on GPUs using programmable pipelines. Holograms of scenes with complex objects are computed in real time for a com-

paratively large holographic video display. Future implementations could use NVIDIA's CUDA parallel computing architecture, which allows shared memory for further efficiency gains. Many fringe fragments share the same view modulation vector. Shared memory will reduce the number of view modulation texture fetches.

A wafel can be extended to produce wavefronts other than those corresponding to points – perhaps corresponding to lines, tilted planes, or spline surfaces – as long as these wavefronts can be computed independently and coherently across multiple wafels.

The current implementation of the algorithm is for horizontal-parallax-only wafels. We have noted that this can be extended to full-parallax wafels and holograms by sampling horizontally and vertically and using two-dimensional variable chirped gratings.

Although the DSC Panoramagram algorithm was implemented on an HPO holographic display, it may be better suited for deep scenes displayed on full-parallax large holographic displays or close-in holographic displays with haptic devices.

5. ACKNOWLEDGMENTS

This work has been supported by the Digital Life, Things That Think, and CELab consortia and the Center for Future Storytelling at the MIT Media Laboratory. The authors gratefully acknowledge the donation of equipment by NVIDIA through their Professor Partnership Program.

REFERENCES

1. D. M. Hoffman, A. R. Girshick, K. Akeley, and M. S. Banks, "Vergence–Accommodation Conflicts Hinder Visual Performance and Cause Visual Fatigue," *Journal of Vision*, 8(3):33, 1-30 (2008).
2. M. Lucente, *Diffraction-Specific Fringe Computation for Electro-Holography*, Ph.D. Dissertation, MIT Dept. of Electrical Engineering and Computer Science, Cambridge MA, (1994).
3. W. Plesniak, M. Halle, V. M. Bove, Jr., J. Barabas, and R. Pappu, "Reconfigurable Image Projection Holograms," *Optical Engineering,* 45(11), 115801 (2006).
4. M. Yamaguchi, H. Hoshino, T. Honda, and N. Ohyama, "Phase Added Stereogram: Calculation of Hologram Using Computer Graphics Technique," *Proc. SPIE Practical Holography VII: Materials and Applications,* 1914, 25-31 (1993).
5. D. Vishwanath, "The Focal Blur Gradient Affects Perceived Absolute Distance," *Perception 37 ECVP Abstract Supplement,* 130 (2008).
6. S. A. Benton and V. M. Bove, Jr., *Holographic Imaging,* John Wiley & Sons, Hoboken NJ, Ch. 19 (2008).
7. Q. Y. J. Smithwick, J. Barabas, D. Smalley, and V. M. Bove, Jr., "Real-Time Shader Rendering of Holographic Stereograms," *Proc. SPIE Practical Holography XXIII: Materials and Applications*, 7233, 723302 (2009).
8. H. Yoshikawa and H. Kameyama, "Integral Holography," *Proc. SPIE Practical Holography X,* 2406, 226-234 (1995).
9. P. St.-Hilaire, *Scalable Optical Architectures for Electronic Holography*, Ph.D. Dissertation, MIT Program in Media Arts and Sciences, Cambridge MA, (1994).
10. S. Marcos, E. Moreno, and R. Navarro, "The Depth-of-Field of the Human Eye from Objective and Subjective Measurements," *Vision Res.*, 39(12), 2039-49 (1999).
11. S. A. Benton and V. M. Bove, Jr., *Holographic Imaging,* John Wiley & Sons, Hoboken NJ, Ch. 14 (2008).
12. W. Plesniak, *Haptic Holography: an Early Computational Plastic,* Ph.D. Dissertation, MIT Program in Media Arts and Sciences, Cambridge MA, (2001).
13. S. A. Benton and V. M. Bove, Jr., *Holographic Imaging,* John Wiley & Sons, Hoboken NJ, Ch. 12 (2008).